A Two-Step Perturbation Technique for Nonuniform Single and Differential Lines

Mykola Chernobryvko, Dries Vande Ginste, *Senior Member, IEEE*, and Daniël De Zutter, *Fellow, IEEE*.

***Abstract*—A novel two-step perturbation technique to analyze nonuniform single and differential transmission lines in the frequency domain is presented. Here, nonuniformities are considered as perturbations with respect to a nominal uniform line, allowing an interconnect designer to easily see what the effect of (unwanted) perturbations might be. Based on the Telegrapher's equations, the proposed approach yields second-order ordinary distributed differential equations with source terms. Solving these equations in conjunction with the pertinent boundary conditions leads to the sought-for currents and voltages along the lines. The accuracy and efficiency of the perturbation technique is demonstrated for a linearly tapered microstrip line and for a pair of coupled lines with random nonuniformities. Moreover, the necessity of adopting a two-step perturbation in order to get a good accuracy is also illustrated.**

***Index Terms*—Interconnect modeling, nonuniform transmission line (NUTL), perturbation, Telegrapher's equations.**

I. Introduction

MODELING of nonuniform transmission lines (NUTL), being part of modern high-speed electronic devices and systems, is often a challenging problem. NUTLs have been widely used in several microwave applications, such as filters [1], impedance transformers [2], directional couplers [3], and very large scale integration (VLSI) interconnections [4]. Also, they are applied for impedance matching [5] and ultra wideband pulse shaping [6]. Since skin, proximity, edge and roughness effects can lead to signal integrity problems at high frequencies [7], transmission lines with (undesirable) nonuniformities must be accurately modeled at the early stage of the design process. Due to the varying per-unit-length (p.u.l.) parameters along the NUTL, the differential equations describing them cannot be solved analytically, except for some special cases [8]–[10].

Modern high-speed electronic devices and systems are characterized by presence of interconnecting networks with nonuniform transmission lines (NUTLs). Modeling of nonuniform single lines, being a part of such interconnecting networks, is often challenging task. The usage of nonuniform single lines are of great interest to the design engineer in many microwave applications such as such as filters [1], impedance transformers [2], directional couplers [3], and very large scale integration (VLSI) interconnections [4]. Moreover, transmission lines with (undesirable) nonuniformities must be accurately modeled at early stage of design process, because skin, proximity, edge, and roughness effects can cause signal integrity problems.

Therefore, plenty of research has been devoted to the numerical solution of nonuniform lines, both in the time and frequency domain. For instance, Precise Time-Step Integration [11] and Differential Quadrature Methods [12] are stable and demonstrate good accuracy, but they are very time consuming. One of the easiest ways to deal with a NUTL is to approximate it as a cascade of discrete uniform transmission lines [13], [14]. Unfortunately, in modern applications, the number of discrete sections of the line must be quite large to accurately account for all nonuniformities and increasing the number of sections reduces the efficiency of the method. Another technique, based on the method of characteristics [15], allows to convert the hyperbolic partial differential equations of the NUTLs into a set of ordinary differential equations. However, to account for frequency-dependent p.u.l. parameters of the lines, convolutions need to be computed [16], again increasing the calculation time. Methods proposed in [17] and [18] use Tailor and Fourier expansions to describe the properties of nonuniform lines, but can only be applied as long as the series converge. Other contributions are based on waveform relaxation, see e.g. [19], congruence transforms, see e.g. [20], or wavelet expansion, see e.g. [21]. In [22] an improved averaging technique for single lines with subwavelength nonuniformities is presented. Finally, [23] presents an equivalent source technique for single lines solving the pertinent integral equation in an iterative way and presenting examples using two iterations.

In this contribution, we propose a two-step frequency-domain perturbation technique for nonuniform single lines. The cross-sectional properties can change in an arbitrary way for such type of lines, allowing to apply our method to a large variety of NUTLs with a single signal conductor with frequency- and place-dependent parameters. We start our technique from considering a *uniform* transmission line in the quasi-TM regime [24], described in terms of the well-known RLGC-matrix, as the nominal structure. Next, the nonuniformities are treated as perturbations with respect to (w.r.t.) these nominal values of the complex inductance and capacitance matrices. Knowing the nominal voltages and currents obtained by solving the classical Telegrapher's equations, we get a first-order perturbation. The solution of the first perturbation step is found by solving the same set of Telegrapher's equations, however in this step, with distributed voltage and current sources depending on the nominal voltages and currents and on the deviation of the RLGC-values from their nominal value in each point along the transmission line. Unfortunately,

M. Chernobryvko, D. Vande Ginste and D. De Zutter are with the Electromagnetics Group, Department of Information Technology, Ghent University, St. Pietersnieuwstraat 41, 9000 Ghent, Belgium (e-mail: mykola.chernobryvko@intec.ugent.be).

the results of the first-order perturbation appear to be not sufficiently precise. To achieve the substantial gain in accuracy, the second perturbation step is introduced. The procedure of the second perturbation step is similar to the previous one, but now accounting voltages and currents of the nominal solution and of the first-order perturbation. The final equations are relatively simple making our two-step perturbation technique very efficient.

In this paper, we propose a novel frequency domain perturbation technique with two perturbation steps, not only for nonuniform single lines but also for the technologically important case of differential lines. For both type of lines, the cross-sectional properties can change in an arbitrary way, allowing to apply our technique to a large number of NUTLs with frequency- and place-dependent line parameters. To construct the presented technique, we start from the well-known RLGC-matrix description of a *uniform* transmission line in the quasi-TM regime [24], which is considered to be the nominal structure. Next, the nonuniformities are treated as perturbations with respect to (w.r.t.) these nominal values of the complex inductance and capacitance matrices. Starting from the knowledge of the nominal voltages and currents obtained by solving the classical Telegrapher's equations, a first-order perturbation is obtained. This first-order perturbation is found by solving the same set of Telegrapher's equations but now with distributed voltage and current sources depending on the nominal voltages and currents and on the deviation of the RLGC-values from their nominal value in each point along the transmission line. However, it turns out that the obtained result is not sufficiently accurate. A substantial gain in accuracy is obtained by repeating the procedure, i.e. by introducing a second perturbation step, which now takes voltages and currents of the nominal solution and of the first-order perturbation into account. Due to the relative simplicity of the final equations, the novel *two-step* perturbation technique is very efficient. Its accuracy and efficiency are demonstrated by applying it to a linearly tapered microstrip line and to a pair of coupled lines with random nonuniformities.

The outline of this paper is as follows. In a first step, we construct the perturbation technique for a single line (Section II). At the end of this section, some remarks are formulated as to the range of applicability of the proposed method. Next, in Section III, the technique is extended to differential lines. The theory is validated and illustrated in Section IV. The examples comprise the application of the proposed technique to a linearly tapered microstrip line (Section IV-A) and to a pair of nonuniform coupled lines (Section IV-B). Finally, conclusions are summarized in Section V.

II. Perturbation solution for a single signal conductor

We will perform our calculations within the framework of the quasi-TM approach and in the frequency domain (with the $e^{j\omega t}$ dependence suppressed) considering a single voltage V and a single current I. To simplify notations we will work with a complex p.u.l. inductance L and capacitance C, i.e. the p.u.l. resistance R and conductance G are understood to be part of L and C ($L = L + \frac{R}{j\omega}$ and $C = C + \frac{G}{j\omega}$). Our starting point are the well-known Telegrapher's equations:

$$\frac{dV(z)}{dz} = -j\omega L(z) I(z), \tag{1}$$

$$\frac{dI(z)}{dz} = -j\omega C(z) V(z), \tag{2}$$

with z the signal propagation direction and where we have explicitly made clear that C and L depend on z. To perform a perturbation analysis, we introduce the following expansions:

$$\begin{aligned} V(z) &= \tilde{V}(z) + \Delta V_1(z) + \Delta V_2(z) + ..., \\ I(z) &= \tilde{I}(z) + \Delta I_1(z) + \Delta I_2(z) + ..., \\ C(z) &= \tilde{C} + \Delta C(z), \\ L(z) &= \tilde{L} + \Delta L(z). \end{aligned} \tag{3}$$

The leading terms of the series expansions (3) for voltage $\tilde{V}(z)$ and current $\tilde{I}(z)$ will be labeled as the *unperturbed* values. The remaining terms are perturbations of order one, two, etc. $C(z)$ and $L(z)$ in (3) are written as the sum of a constant part and a place-dependent part without extention in series. Here, $\tilde{C}$ and $\tilde{L}$ are the unperturbed values of the p.u.l. capacitance and inductance. $\Delta C(z)$ and $\Delta L(z)$ are the variations of the capacitance and inductance along the line which remain when subtracting the constant values $\tilde{C}$ and $\tilde{L}$ from $C(z)$ and $L(z)$ respectively. Remark that $\tilde{C}$ and $\tilde{L}$ are not necessarily the mean values of C and L over the line. We only suppose that $\Delta C(z)$ and $\Delta L(z)$ are small enough with respect to $\tilde{C}$ and $\tilde{L}$. Substituting (3) into (1) and (2) and collecting terms of the same order, yields

$$\frac{d\tilde{V}(z)}{dz} = -j\omega \tilde{L} \tilde{I}(z), \tag{4}$$

$$\frac{d\tilde{I}(z)}{dz} = -j\omega \tilde{C} \tilde{V}(z), \tag{5}$$

$$\frac{d\Delta V_1(z)}{dz} = -j\omega \tilde{L} \Delta I_1(z) - j\omega \Delta L(z) \tilde{I}(z), \tag{6}$$

$$\frac{d\Delta I_1(z)}{dz} = -j\omega \tilde{C} \Delta V_1(z) - j\omega \Delta C(z) \tilde{V}(z), \tag{7}$$

$$\frac{d\Delta V_2(z)}{dz} = -j\omega \tilde{L} \Delta I_2(z) - j\omega \Delta L(z) \Delta I_1(z), \tag{8}$$

$$\frac{d\Delta I_2(z)}{dz} = -j\omega \tilde{C} \Delta V_2(z) - j\omega \Delta C(z) \Delta V_1(z). \tag{9}$$

Higher-order perturbations could be obtained in a similar way. From this point on, for ease of notation, the argument z will be omitted. The solutions of (4) and (5) are straightforward:

$$\tilde{V} = Ae^{-jk_0 z} + Be^{+jk_0 z}, \tag{10}$$

$$\tilde{I} = \frac{1}{Z_0}(Ae^{-jk_0 z} - Be^{+jk_0 z}), \tag{11}$$

with the unperturbed characteristic impedance $Z_0 = \sqrt{\tilde{L}/\tilde{C}}$ and the unperturbed wave number $k_0 = \omega\sqrt{\tilde{L}\tilde{C}}$. At this point we introduce the boundary conditions. We will consider a signal conductor of length l terminated in a load Z_L and excited by a Thévenin source V_g with internal impedance Z_g. Contrary to what is often done in transmission line theory, the

load will be placed at $z = l$ and the source at $z = 0$. These boundary conditions lead to

$$A = \frac{V_g}{1 + \frac{Z_g}{Z_0}} \frac{1}{1 - K_L K_g e^{-2jk_0 l}}, \tag{12}$$

$$B = K_L A e^{-2jk_0 l}, \tag{13}$$

with the reflection coefficients K_L and K_g at the load and at the generator, respectively, given by:

$$K_L = \frac{Z_L - Z_0}{Z_L + Z_0},$$
$$K_g = \frac{Z_g - Z_0}{Z_g + Z_0}. \tag{14}$$

From (6) and (7), the first-order perturbation ΔV_1 satisfies

$$\frac{d^2 \Delta V_1}{dz^2} + k_0^2 \Delta V_1 = -k_0^2 \tau_C \tilde{V} - jk_0 \frac{d}{dz}(\tau_L Z_0 \tilde{I}), \tag{15}$$

with $\tau_C = \frac{\Delta C}{\tilde{C}}$ and $\tau_L = \frac{\Delta L}{\tilde{L}}$. Analogically, (8) and (9) give us

$$\frac{d^2 \Delta V_2}{dz^2} + k_0^2 \Delta V_2 = -k_0^2 \tau_C \Delta V_1 - jk_0 \frac{d}{dz}(\tau_L Z_0 \Delta I_1). \tag{16}$$

The above differential equations (15) and (16) can now be solved by applying the general theory for second-order differential equations with an arbitrary source term, see e.g. [1] or the Appendix A of [23]. The solutions take the following form :

$$\Delta V_i = C_i e^{-jk_0 z} + D_i e^{+jk_0 z} + \Delta V_{ip}, \tag{17}$$

$$Z_0 \Delta I_i = C_i e^{-jk_0 z} - D_i e^{+jk_0 z} + Z_0 \Delta I_{ip}. \tag{18}$$

with $i = 1, 2$. The particular solutions ΔV_{ip} and ΔI_{ip} can be written as

$$\Delta V_{ip}(z) = -\frac{jk_0}{2} \left[F_i(z) e^{-jk_0 z} + G_i(z) e^{+jk_0 z} \right], \tag{19}$$

$$Z_0 \Delta I_{ip}(z) = -\frac{jk_0}{2} \left[F_i(z) e^{-jk_0 z} - G_i(z) e^{+jk_0 z} \right]. \tag{20}$$

The values of F_1 and G_1 for the first-order perturbation are given by

$$F_1(z) = \gamma A + \beta B, \quad G_1(z) = -(\alpha A + \gamma B), \tag{21}$$

where A and B are given in (12) and (13) respectively and with

$$\alpha(z) = \int_0^z [\tau_C(z') - \tau_L(z')] e^{-2jk_0 z'} dz', \tag{22}$$

$$\beta(z) = \int_0^z [\tau_C(z') - \tau_L(z')] e^{+2jk_0 z'} dz', \tag{23}$$

$$\gamma(z) = \int_0^z [\tau_C(z') + \tau_L(z')] dz'. \tag{24}$$

Also, for the second-order perturbation the values of F_2 and G_2 are found to be

$$F_2(z) = \gamma C_1 + \beta D_1 - \frac{jk_0}{2}(\delta_1 A + \delta_2 B) + \frac{jk_0}{2}(\delta_3 A + \delta_4 B),$$
$$G_2(z) = -\alpha C_1 - \gamma D_1 + \frac{jk_0}{2}(\delta_5 A + \delta_6 B) - \frac{jk_0}{2}(\delta_7 A + \delta_1 B), \tag{25}$$

with

$$\delta_1(z) = \int_0^z [\tau_C(z') + \tau_L(z')] \gamma(z') dz', \tag{26}$$

$$\delta_2(z) = \int_0^z [\tau_C(z') + \tau_L(z')] \beta(z') dz', \tag{27}$$

$$\delta_3(z) = \int_0^z [\tau_C(z') - \tau_L(z')] \alpha(z') e^{+2jk_0 z'} dz', \tag{28}$$

$$\delta_4(z) = \int_0^z [\tau_C(z') - \tau_L(z')] \gamma(z') e^{+2jk_0 z'} dz', \tag{29}$$

$$\delta_5(z) = \int_0^z [\tau_C(z') - \tau_L(z')] \gamma(z') e^{-2jk_0 z'} dz', \tag{30}$$

$$\delta_6(z) = \int_0^z [\tau_C(z') - \tau_L(z')] \beta(z') e^{-2jk_0 z'} dz', \tag{31}$$

$$\delta_7(z) = \int_0^z [\tau_C(z') + \tau_L(z')] \alpha(z') dz'. \tag{32}$$

As can be seen from (21)-(32) $F_i(z = 0) = 0$ and $G_i(z = 0) = 0$. The unknown coefficients C_i and D_i of (17) and (18) are found by enforcing the following boundary conditions:

$$\Delta V_i(z = 0) = -Z_g \Delta I_i(z = 0), \tag{33}$$

$$\Delta V_i(z = l) = Z_L \Delta I_i(z = l). \tag{34}$$

Note that the source V_g itself drops out in the perturbed boundary conditions. Indeed, as already $\tilde{V}(z = 0) = -Z_g \tilde{I}(z = 0) + V_g$ and as this boundary condition must also remain satisfied by the total voltage and current, it follows that ΔV_i and ΔI_i must satisfy (33) and (34). As $F_i(z = 0) = G_i(z = 0) = 0$, the first boundary condition immediately yields $C_i = K_g D_i$. The second boundary condition then leads to

$$D_i = \frac{[Z_L \Delta I_{ip}(z = l) - \Delta V_{ip}(z = l)] e^{-jk_0 l}}{(1 + \frac{Z_L}{Z_0})(1 - K_L K_g e^{-2jk_0 l})}. \tag{35}$$

At this point the following remark is important. The final expressions for ΔV_{ip} and ΔI_{ip} depend on $\alpha(z)$, $\beta(z)$ and $\gamma(z)$ (see Appendix **??**). It is now possible to simplify these expressions by explicitly choosing $\gamma(z = l)$ to be zero. This can be achieved by choosing $\tilde{C}$ and $\tilde{L}$ to be the mean values over the line of $C(z)$ and $L(z)$, respectively. This is the option that was also taken in [23]. However, we have chosen to derive our expressions for the more general case aiming at applications that might be of particular interest to high-speed designers. In high-speed design, a nominal L_{nom} and C_{nom} will typically have been selected according to the wanted impedance level and the used substrate technology. From this point of view, it might be preferable to take these nominal design values as the unperturbed ones, i.e. $\tilde{L} = L_{nom}$ and $\tilde{C} = C_{nom}$, to next evaluate the effect of variations of these nominal values due to the manufacturing process. In such a case $\gamma(z = l)$ will not be zero. As will become clear from the numerical results, adding a second-order perturbation greatly improves the accuracy. For an intuitive understanding of the reason for this, we refer the reader to Section IV. Note that, in the single line analysis of [23], the first iteration corresponds to what is above called the unperturbed case, but only provided $\gamma(z = l)$ is selected to be zero. The second iteration in [23] then corresponds to what we call the first perturbation step.

As pointed out by the reviewers, further research is needed to find out if it is possible to derive hard mathematical conditions under which this second-order perturbation (or higher-order ones) will always increase accuracy. We have not yet been able to produce such a proof under general circumstances. Nevertheless, from an engineering point of view, and as confirmed by the examples given in this paper and by many others we used to verify our theory, it is obvious that when the variation of $L(z)$ and $C(z)$ remains reasonable, a very good accuracy is obtained. It is interesting to mention that (12) and (35) indicate that high K_L and/or K_g values should be avoided because the unperturbed solution will then exhibit a high voltage standing wave pattern. With typical applications in high-speed design in mind, such highly non-matched lines will rarely occur.

III. Perturbation solution for a differential line pair

In this section we turn to the analysis of the differential line pair (see Fig. 5 for an example of a differential microstrip line). The Telegrapher's equations now become:

$$\frac{d\mathcal{V}(z)}{dz} = -j\omega\mathcal{L}(z)\mathcal{I}(z), \tag{36}$$

$$\frac{d\mathcal{I}(z)}{dz} = -j\omega\mathcal{C}(z)\mathcal{V}(z). \tag{37}$$

$\mathcal{V} = [V_1\ V_2]^T$ and $\mathcal{I} = [I_1\ I_2]^T$ are the voltage and current column vectors, holding the two voltages and two currents along the lines, while $\mathcal{C}$ and $\mathcal{L}$ are the 2×2 symmetric p.u.l. capacitance and inductance matrices. All quantities can be expanded in a completely analogous way as in (3) and differential equations similar to (4)-(9) are readily obtained. The unperturbed p.u.l. C- and L-matrices are z-independent and can be written as:

$$\tilde{\mathcal{C}} = \begin{pmatrix} C_a & -C_b \\ -C_b & C_a \end{pmatrix} \qquad \tilde{\mathcal{L}} = \begin{pmatrix} L_a & L_b \\ L_b & L_a \end{pmatrix}. \tag{38}$$

Due to the well-known properties of such matrices [25], C_a, C_b, L_a and L_b in (38) are positive. Let us first take a closer look at the solution of the unperturbed problem. It is well-known [26] that this solution consists of an even and an odd mode contribution, i.e.:

$$\begin{aligned} \tilde{V}_1(z) &= [\tilde{V}_e(z) + \tilde{V}_o(z)]/2 \quad & \tilde{V}_2(z) &= [\tilde{V}_e(z) - \tilde{V}_o(z)]/2, \\ \tilde{I}_1(z) &= [\tilde{I}_e(z) + \tilde{I}_o(z)]/2 \quad & \tilde{I}_2(z) &= [\tilde{I}_e(z) - \tilde{I}_o(z)]/2. \end{aligned} \tag{39}$$

Often, the designations common and differential mode are used, replacing the couples $(\tilde{V}_e, \tilde{I}_e)$ and $(\tilde{V}_o, \tilde{I}_o)$ by $(\tilde{V}_e/2, \tilde{I}_e)$ and $(\tilde{V}_o, \tilde{I}_o/2)$. The unperturbed differential equations for the even and odd mode are easily found to be

$$\begin{aligned} \frac{d\tilde{V}_e(z)}{dz} &= -j\omega(L_a + L_b)\tilde{I}_e(z), \\ \frac{d\tilde{I}_e(z)}{dz} &= -j\omega(C_a - C_b)\tilde{V}_e(z), \\ \frac{d\tilde{V}_o(z)}{dz} &= -j\omega(L_a - L_b)\tilde{I}_o(z), \\ \frac{d\tilde{I}_o(z)}{dz} &= -j\omega(C_a + C_b)\tilde{V}_o(z). \end{aligned} \tag{40}$$

Hence, the modal voltages become:

$$\begin{aligned} \tilde{V}_e &= (A_1 e^{-jk_e z} + B_1 e^{+jk_e z}), \\ \tilde{V}_o &= (A_2 e^{-jk_o z} + B_2 e^{+jk_o z}). \end{aligned} \tag{41}$$

Even and odd mode wave numbers k_e and k_o are given by:

$$\frac{k_e}{\omega} = \sqrt{(L_a + L_b)(C_a - C_b)}, \frac{k_o}{\omega} = \sqrt{(L_a - L_b)(C_a + C_b)}. \tag{42}$$

The corresponding modal currents are

$$\begin{aligned} \tilde{I}_e &= (A_e e^{-jk_e z} - B_e e^{+jk_e z})/Z_e, \\ \tilde{I}_o &= (A_o e^{-jk_o z} - B_o e^{+jk_o z})/Z_o, \end{aligned} \tag{43}$$

with the even and odd mode impedances given by

$$Z_e = \sqrt{\frac{L_a + L_b}{C_a - C_b}}, \quad Z_o = \sqrt{\frac{L_a - L_b}{C_a + C_b}}. \tag{44}$$

Remark that the common mode and differential mode impedances are given by $Z_c = Z_e/2$ and $Z_d = 2Z_o$. To determine to unknown coefficients A_e, A_o, B_e and B_o, the boundary conditions at $z = 0$ and $z = l$ must be enforced. Referring to the very general source and load conditions shown in Figs. 1 and 2, the detailed expressions for these boundary conditions in terms of even and odd mode voltages and currents are given in Appendix **??**.

Before turning to the first-order perturbation, let us take a closer look at $\Delta\mathcal{C}$ and $\Delta\mathcal{L}$. $\Delta\mathcal{C}$ can be written as

$$\Delta\mathcal{C} = \begin{pmatrix} \Delta C_{a1} & -\Delta C_b \\ -\Delta C_b & \Delta C_{a2} \end{pmatrix}. \tag{45}$$

As $\tilde{\mathcal{C}} + \Delta\mathcal{C}$ must have all the properties of a proper capacitance matrix in each point along the line pair, it can be asserted that the above matrix is symmetric but the entries of the matrix can *either* be *positive* or *negative*. As will become clear below, it is useful to rewrite (45) as:

$$\begin{aligned} \Delta\mathcal{C} &= \begin{pmatrix} \frac{\Delta C_{a1} + \Delta C_{a2}}{2} & -\Delta C_b \\ -\Delta C_b & \frac{\Delta C_{a1} + \Delta C_{a2}}{2} \end{pmatrix} \\ &+ \begin{pmatrix} \frac{\Delta C_{a1} - \Delta C_{a2}}{2} & 0 \\ 0 & -\frac{\Delta C_{a1} - \Delta C_{a2}}{2} \end{pmatrix}. \end{aligned} \tag{46}$$

and

$$\begin{aligned} \Delta\mathcal{L} &= \begin{pmatrix} \frac{\Delta L_{a1} + \Delta L_{a2}}{2} & \Delta L_b \\ \Delta L_b & \frac{\Delta L_{a1} + \Delta L_{a2}}{2} \end{pmatrix} \\ &+ \begin{pmatrix} \frac{\Delta L_{a1} - \Delta L_{a2}}{2} & 0 \\ 0 & -\frac{\Delta L_{a1} - \Delta L_{a2}}{2} \end{pmatrix}. \end{aligned} \tag{47}$$

With (46) and (47), the differential equations for the even and odd mode *first-order perturbation*, become

$$\begin{aligned} \frac{d\Delta V_{1e}}{dz} &= -j\omega(L_a + L_b)\Delta I_{1e} - j\omega(l_a + l_b)\tilde{I}_e - j\omega l\tilde{I}_o, \\ \frac{d\Delta I_{1e}}{dz} &= -j\omega(C_a - C_b)\Delta V_{1e} - j\omega(c_a - c_b)\tilde{V}_e - j\omega c\tilde{V}_o, \\ \frac{d\Delta V_{1o}}{dz} &= -j\omega(L_a - L_b)\Delta I_{1o} - j\omega(l_a - l_b)\tilde{I}_o - j\omega l\tilde{I}_e, \\ \frac{d\Delta I_{1o}}{dz} &= -j\omega(C_a + C_b)\Delta V_{1o} - j\omega(c_a + c_b)\tilde{V}_o - j\omega c\tilde{V}_e, \end{aligned} \tag{48}$$

with

$$c_a = \frac{\Delta C_{a1} + \Delta C_{a2}}{2}, \quad c_b = \Delta C_b, \quad c = \frac{\Delta C_{a1} - \Delta C_{a2}}{2}$$
$$l_a = \frac{\Delta L_{a1} + \Delta L_{a2}}{2}, \quad l_b = \Delta L_b, \quad l = \frac{\Delta L_{a1} - \Delta L_{a2}}{2} \tag{49}$$

Equations (48) exhibit the same structure as their single line counterparts (6) and (7). In the differential line case we have a separate set of equations for the two modes: the even mode comes with the $(C_a - C_b, L_a + L_b)$ p.u.l. set; the odd mode with the $(C_a + C_b, L_a - L_b)$ p.u.l. set. In each of the equations, two source terms can be distinguished: one source term due to each mode, i.e. the source terms are responsible for *mode coupling*! By rewriting $\Delta\mathcal{C}$ and $\Delta\mathcal{L}$ as in (46) and (47), it becomes clear which part of the variation of the capacitance and inductance along the line is responsible for perturbation with and without mode coupling. Given the similarity between the single line case and the differential line case, when viewed as a superposition of even and odd mode, the actual solution of (40) proceeds along the same lines as sketched in Section II. Two pairs of unknown coefficient will have to be introduced (C_e, D_e, C_o and D_o in the notation of Section II). They can be determined by enforcing boundary conditions (**??**) in which the sources are left out and unperturbed quantities are replaced by first order perturbations. Integrals similar to (22) and (23) will appear in the final solution, but instead of the $e^{\pm 2jk_0 z}$ exponentials, $e^{\pm 2jk_o z}$, $e^{\pm 2jk_e z}$, $e^{\pm 2j(k_o - k_e)z}$ and $e^{\pm 2j(k_o + k_e)z}$ exponentials will now appear. Following (24) it turned out that for the unperturbed value of the p.u.l. capacitance $\tilde{\mathcal{C}}$ and its inductive counterpart $\tilde{\mathcal{L}}$, the mean value of $\mathcal{C}(z)$ and $\mathcal{L}(z)$ can, but do not have to, be used. Similar choices, simplifying the calculations, are possible for the differential line case. To this end, $2C_a$ in (38) should be chosen to be the mean value of $C_{11}(z) + C_{22}(z)$, while C_b must be put equal to the mean value of $|C_{12}(z)| = |C_{21}(z)|$ with C_{11}, C_{12}, C_{21} and C_{22} the elements of the z-dependent 2×2 p.u.l. capacitance matrix $\mathcal{C} = \tilde{\mathcal{C}} + \Delta\mathcal{C}$ and similarly for the choices of $2L_a$ and L_b. It is, however, also possible to choose the nominal design values for $\tilde{\mathcal{C}}$ and $\tilde{\mathcal{L}}$, as such allows the high-speed designer to assess the influence of the unwanted perturbations on his/her design.

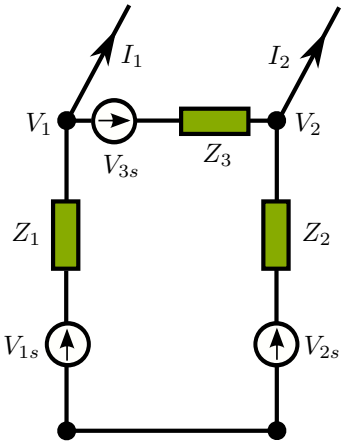

Fig. 1. Excitation of the differential line pair.

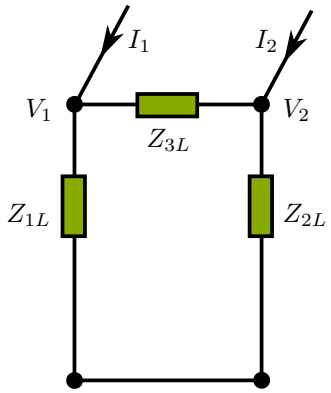

Fig. 2. Termination of the differential line pair.

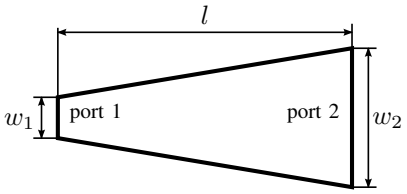

Fig. 3. Top view of a linearly tapered microstrip line.

IV. Numerical results

A. Linearly Tapered Microstrip Line

The aforementioned technique for a single TL is validated by means of comparison with the approach described in [9]. The analytical model for lossy linearly tapered microstrip lines (LTML) of [9] thereby acts as an exact reference solution. This model results from a quasi-TEM approximation which is a special case of the more general quasi-TM approximation in [24]. The top view of the investigated structure is shown in Fig. 3. It concerns a tapered microstrip line of length $l = 50$ mm, residing on a RO4350B substrate with a thickness $h = 1.524$ mm, a relative permittivity $\varepsilon_r = 3.66$ and a loss tangent $\tan\delta = 0.003$. The metal thickness and conductivity of the taper are $t = 35$ μm and $\sigma = 5.8{\cdot}10^7$ S/m, respectively. The line width w_1 at port 1 is kept constant at 3 mm, while the width w_2 is a parameter in our study. Approximate models for the varying complex p.u.l. capacitance $C(z)$ and p.u.l. inductance $L(z)$ along the line are calculated with the technique described in [9], which leads to an analytical solution, based on Airy functions.

First, we compute the S-parameters for this tapered line, w.r.t. 50 Ω reference impedances at both ports, using the analytical solution and the novel perturbation technique with the two perturbation steps. The obtained absolute value of the S-parameters are depicted in Fig. 4 for the case that $w_2 = 4$ mm. From this figure, the high accuracy of the novel technique is appreciated. In addition, the S-parameters of the uniform, non-perturbed line, i.e. when $w_2 = 3$ mm, are also

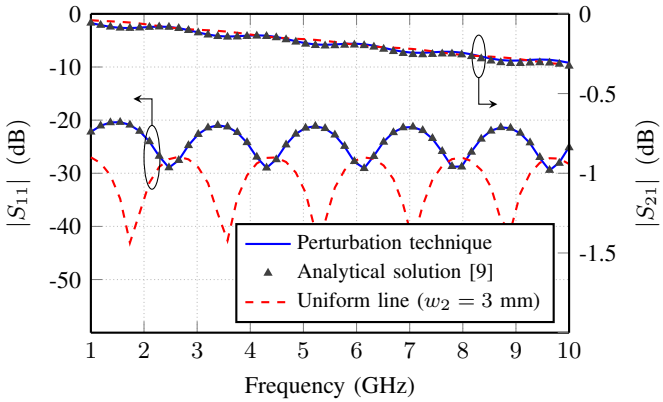

Fig. 4. Magnitude of S_{11} and S_{21} as a function of frequency for the tapered line of Fig. 3 with $w_1 = 3$ mm, $w_2 = 4$ mm and $l = 50$ mm, using the novel perturbation technique with two perturbation steps and the analytical reference solution [9]. To indicate the influence of the tapering, the S-parameters of a uniform line with $w_1 = w_2 = 3$ mm are also shown.

TABLE I
INFLUENCE OF VARYING THE WIDTH w_2 ($w_1 = 3$ mm, $l = 50$ mm)

w_2 (mm)	Maximum $\Delta L(z)$ (%)	Maximum $\Delta C(z)$ (%)	ΔS_{21} @ 10 GHz (%)
1	65.7	43.9	3.35
1.5	40.8	32.4	1.18
2	23.4	21.4	0.37
2.5	10.3	10.6	0.07
3	0	0	0
3.5	8.4	10.5	0.06
4	15.4	21.1	0.23
4.5	21.3	31.8	0.51
5	26.4	42.2	0.90

shown, clearly illustrating the influence of the tapering.

Obviously, the novel approach is intended for NUTLs for which the nonuniformities can be considered as perturbations w.r.t. a nominal case, i.e. for cases in which ΔL and ΔC are not too large. Therefore, second, to clearly demonstrate and to quantify the accuracy of our technique as well as illustrating its limitations, a parameter study is performed. We define the relative error on S_{21} (taking both magnitude and phase into account) as follows:

$$\Delta S_{21} = \left| \frac{S_{21}^{(a)} - S_{21}^{(p)}}{S_{21}^{(a)}} \right|, \tag{50}$$

where $S_{21}^{(a)}$ is the analytical result and $S_{21}^{(p)}$ is obtained by means of our perturbation technique with the two perturbation steps. Table I shows how changing the width w_2 influences the maximum variations of capacitance and inductance, expressed in percent w.r.t. the nominal values, and it shows the relative error ΔS_{21} at 10 GHz. As can be seen from Table I, if ΔL and ΔC increase, ΔS_{21}, obviously, grows too. However, even for a ΔL and ΔC up to 30% w.r.t. the nominal values, for this example, the relative error remains limited to about 0.5%. The results in Table I are given for the highest considered frequency (i.e. 10 GHz). For lower frequencies the errors decrease.

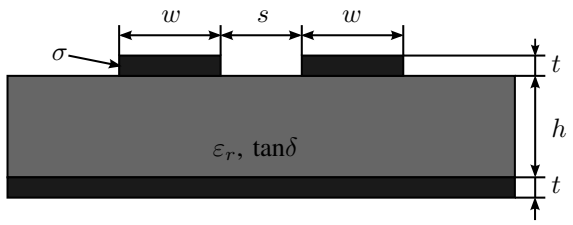

Fig. 5. Nominal cross-section of the two coupled microstrip lines with $w = 1.8$ mm, $s = 700$ μm, $h = 1.524$ mm, $t = 35$ μm, $\sigma = 5.8{\cdot}10^7$ S/m, $\varepsilon_r = 3.66$ and $\tan\,\delta = 0.003$.

Third, of course, the electrical length of the line also plays an important role, as phase errors can accumulate. For the taper of Fig. 3, which is already rather long, i.e. 50 mm at 10 GHz, the perturbation technique gives a relative error equal to 0.23% when $w_2 = 4$ mm (see Table I). The relative error increases to 0.98% for an even longer taper with length $l = 100$ mm. For a shorter taper with $l = 25$ mm, the relative error becomes very small, i.e. 0.05%.

B. Nonuniform Coupled Lines

For this next example, we focus on a pair of coupled lines. The nominal cross-section of this pair is the one also used in [27] and it is shown in Fig. 5. The track width is $w = 1.8$ mm, the spacing between the lines is $s = 700$ μm. The microstrip lines and the ground plane have a thickness $t = 35$ μm and a conductivity $\sigma = 5.8{\cdot}10^7$ S/m. The parameters of the substrate are the same as for the LTML described in the previous subsection and the lines are given a length $l = 50$ mm. For this uniform transmission line, which is considered to be the nominal structure, the nominal frequency dependent $\tilde{\mathcal{L}}$- and $\tilde{\mathcal{C}}$-matrices are calculated with the technique of [24], [28]. This technique is a 2-D electromagnetic numerical method that assumes a quasi-TM behavior of the fields and that in essence solves the pertinent complex capacitance and complex inductance problem. By introducing a differential surface admittance operator, these two problems are cast as boundary integral equations, which can be solved efficiently and accurately. For further details on the usage of this method we refer the reader to [29] and the references therein.

Now, random nonuniformities are introduced by dividing the 50 mm lines into 100 equal sections, and for each section the p.u.l. parameters are varied by multiplying each matrix element L_{11}, L_{22}, $L_{12} = L_{21}$, C_{11}, C_{22} and $C_{12} = C_{21}$ of $\tilde{\mathcal{L}}$ and $\tilde{\mathcal{C}}$ with a random variable (RV) that is uniformly distributed within the interval [1 - ξ, 1 + ξ]. The six RVs so used are independent of each other. The number ξ determines the maximum deviation from the nominal case and it is a parameter of our study. As a reference solution we use the chain parameter matrix approach described in [13]. Based on Telegrapher's equations for each individual section, the voltages and currents at the output of this section are related to the voltages and currents at its input by means of a 4×4 chain parameter matrix. The overall chain parameter matrix of the entire interconnect structure is then obtained as a product of the 100 chain parameter matrices of the individual

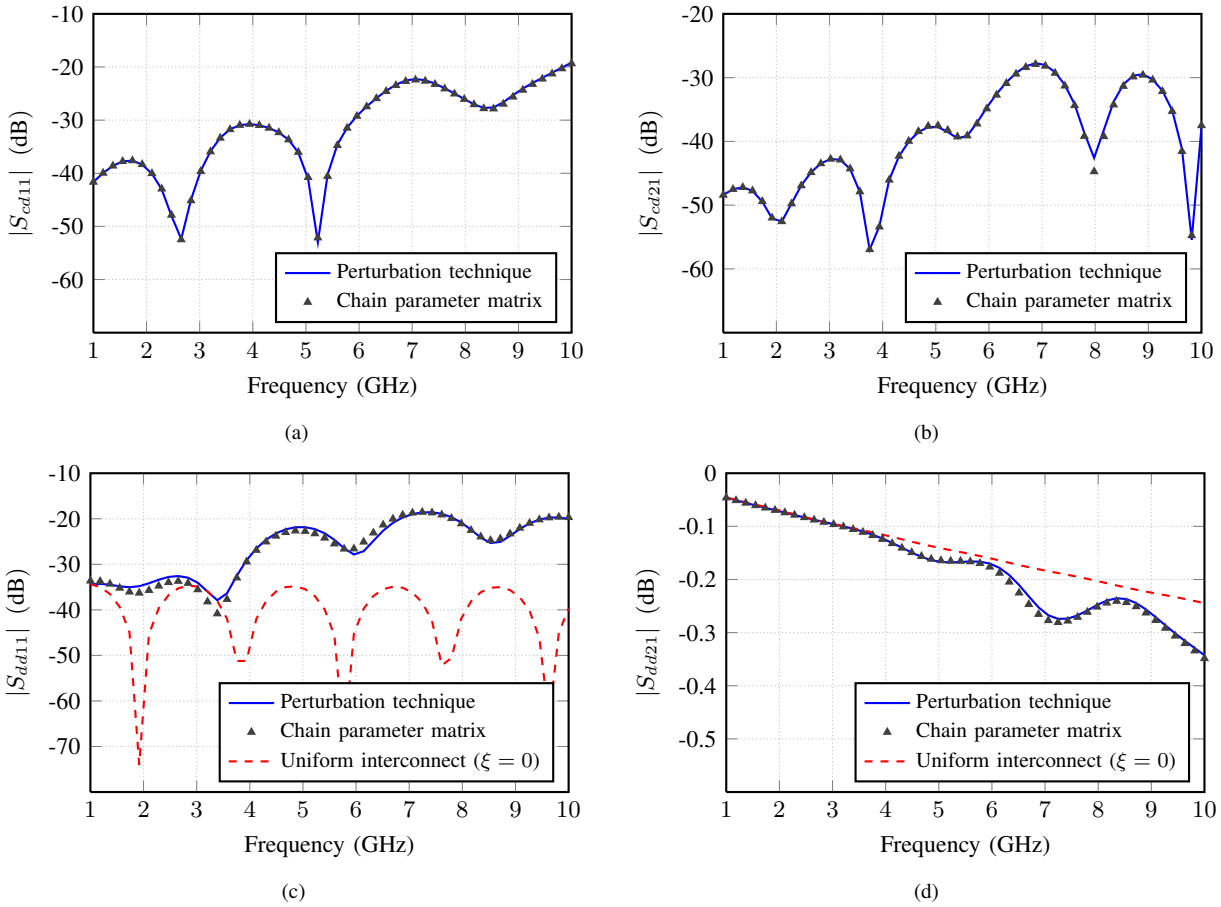

Fig. 6. Modal S-parameters of the pair of coupled lines for the case when the maximum variation of p.u.l. capacitance and inductance is $\xi = 20\%$, using the *two-step* perturbation and the chain parameter matrix techniques. (a) Backward differential-to-common mode conversion. (b) Forward differential-to-common mode conversion. (c) Differential mode reflection coefficient. (d) Differential mode transmission coefficient. To indicate the influence of the perturbation, the S-parameters of the nominal, uniform line ($\xi = 0$) are also shown in (c) and (d).

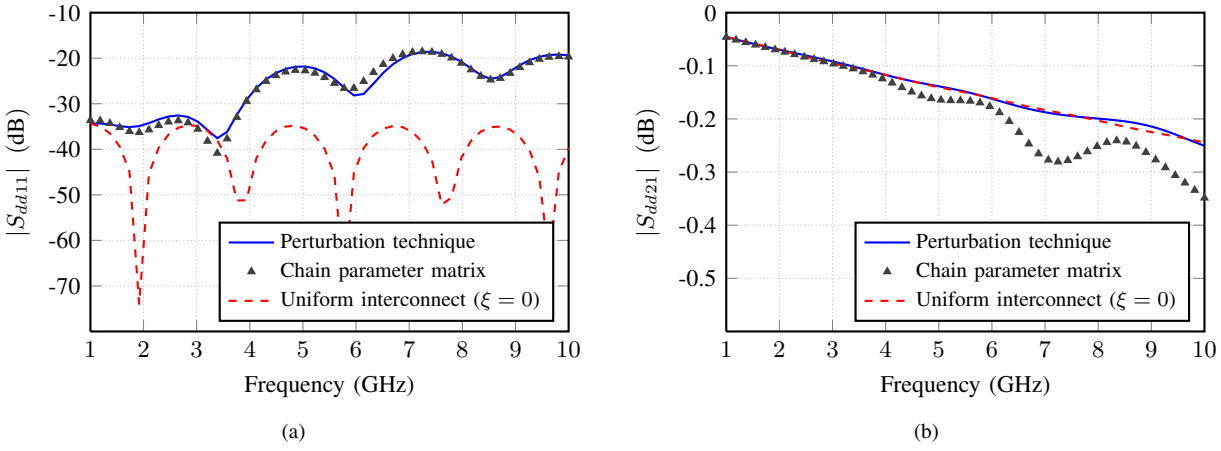

Fig. 7. Differential mode reflection (a) and transmission (b) coefficients of the pair of coupled lines for the case when the maximum variation of p.u.l. capacitance and inductance is $\xi = 20\%$, using the *one-step* perturbation and the chain parameter matrix techniques.

sections. From this overall chain parameter matrix, the 4×4 S-parameter matrix can be easily derived.

We present the results of the novel perturbation technique and the reference solution by means of mixed-mode S-parameters, characterizing the nonuniform pair of coupled lines in terms of the response to common and differential mode signals [30] w.r.t. 50 Ω references impedances, i.e. $Z_1 = Z_2 = Z_{1L} = Z_{2L} = 50\ \Omega$ and Z_3 and Z_{3L} are open circuits (see Figs. 1 and 2). Since transmission of a differential signal is the most interesting for practical applications, Fig. 6 shows the magnitude of the differential-to-common mode conversions S_{cd11} and S_{cd21}, the differential reflection coefficient S_{dd11}

and the differential transmission coefficient S_{dd21}, when the maximum variations are $\xi = 20\%$ w.r.t. the nominal values of the $\tilde{\mathcal{L}}$- and $\tilde{\mathcal{C}}$- matrices' elements. We can see from Fig. 6 that, these mixed-mode S-parameters are captured with a very high accuracy by our novel method. As was also done in the previous example, in Figs. 6 (c) and (d), the magnitude of the reflection coefficient S_{dd11} and the transmission coefficient S_{dd21} of the differential line with the nominal $\tilde{\mathcal{L}}$ and $\tilde{\mathcal{C}}$ along the line are also shown to demonstrate the influence of the random perturbations. Obviously, there is no mode conversion for the uniform, symmetric line of Fig. 5, and hence, this is not shown in Figs. 6 (a) and (b).

At this point, it is instructive to demonstrate the importance of adopting a *two-step* perturbation. In Figs. 7 (a) and (b), the results for $|S_{dd11}|$ and $|S_{dd21}|$ are shown when using a one-step perturbation. It is clearly observed that this might be sufficient for predicting the S-parameters at the near end (Fig. 7 (a)). However, it clearly fails to capture the influence of the variation of the p.u.l. parameters along the line at the far end (Fig. 7 (b)), leading to an $|S_{dd21}|$ that still closely resembles the results for the nominal line. The reader might wonder why the second perturbation step leads to considerable improvements for the transmission parameter, while the reflection result is only slightly affected and is already quite good after the first-order perturbation. An intuitive understanding (here given for a single line) can be obtained when considering a situation for which the nominal problem is already quite well adapted at its terminals, implying that the nominal solution is dominated by a voltage and a current wave travelling in the positive z-direction with phase dependence e^{-jk_0z}. In the first-order perturbation, at a particular point z_0 along the line, this wave will give rise to a voltage source term proportional to $\frac{\Delta C}{C}e^{-jk_0z_0}$ and a current source term proportional to $\frac{\Delta L}{L}e^{-jk_0z_0}$. If the signal originating from these sources travels back to the near-end of the line, an extra phase factor $e^{-jk_0z_0}$ is added. This effect is mathematically expressed through integrals of the type α (22) and β (23). If, however, the same signal travels to the far-end of the line, an extra phase factor $e^{-jk_0(l-z_0)}$ is added, leading to a total phase of e^{-jk_0l}, independent of z_0. Hence, under the considered circumstances, all source contributions in the first-order perturbation are in-phase at the far-end of the line, as mathematically expressed by integral of the type γ (24). When we select our nominal LC-values as the mean value over the line, i.e. $\gamma = 0$, it becomes clear that the first-order perturbation has little influence at the far-end. A second-order perturbation remedies the problem.

Adopting the *two-step* approach again, apart from the magnitude of the S-parameters, accurate results for the phase are obtained as well. This will be demonstrated now, and at the same time, the limitations of the method will be illustrated. Thereto, we calculate the relative error on the transmission coefficient S_{dd21}. The relative error is defined in a similar way as it was done for the LTML, accounting for both its magnitude and phase:

$$\Delta S_{dd21} = \left| \frac{S_{dd21}^{(ch)} - S_{dd21}^{(p)}}{S_{dd21}^{(ch)}} \right|, \tag{51}$$

TABLE II
INFLUENCE OF VARYING THE MAXIMAL VALUE OF $\Delta\mathcal{L}$ AND $\Delta\mathcal{C}$

Max. deviation (%)	ΔS_{dd21} @ 6.6 GHz (%)
10	0.05
15	0.1
20	0.17
25	0.29
30	0.41
35	0.58
40	0.79
45	1.04
50	1.34

TABLE III
CPU TIME COMPARISON

Number of sections	Perturbation technique	Reference solution	Speed-up factor
50	1.56 s	6.48 s	4.15
100	1.88 s	12.68 s	6.74
200	2.52 s	25.15 s	9.98
500	4.49 s	66.23 s	14.75

where $S_{dd21}^{(ch)}$ and $S_{dd21}^{(p)}$ are obtained by means of the chain parameter matrix and perturbation technique respectively. The relative errors were calculated for the entire frequency range up to 10 GHz in order to determine the frequency for which the relative error is the highest. It was found that the highest relative error on S_{dd21} occurs at a frequency of 6.6 GHz. Table II shows that increasing the maximal values of $\Delta\mathcal{L}$ and $\Delta\mathcal{C}$, i.e. increasing ξ, makes the relative error larger. Nevertheless, as can be seen, the relative error remains limited to 1% if perturbations do not exceed 40% w.r.t. the nominal case.

Finally, to demonstrate the efficiency of our novel technique, we consider the computation time of the code in Matlab R2009a. All calculations were performed on a computer with an Intel(R) Core(TM) Quad CPU Q9650 and 8 GB of installed memory (RAM). For the perturbation technique, the computational cost is attributed to the calculation of the integrals (22), (23) and (24) given in Appendix **??**. For the reference technique, the computational complexity scales with the number of sections one uses, and hence, it is less efficient than the newly proposed method. This is demonstrated in Table III, where the computation time is shown for 200 frequency samples (linearly spaced between 1 and 10 GHz) and for a varying number of sections. For example, in the case of 200 sections, we achieve a speed-up of about 10. This speed-up factor becomes even larger if we need to describe the variation of $\Delta\mathcal{L}$ and $\Delta\mathcal{C}$ along the line with more precision, i.e. when increasing the number of sections. Indeed, note that the chain parameter matrix approach always introduces a staircasing effect, this in contrast to the novel perturbation technique presented in this paper.

V. Conclusion

In this paper, a novel perturbation technique has been presented to analyze nonuniform single and differential transmission lines in the frequency domain. Nonuniformities were represented as perturbations w.r.t. a nominal configuration as such allowing to easily see the effect of (unwanted) perturbation during interconnect design. Starting from the Telegrapher's equations and applying two consecutive perturbations, leads to second order differential equations, describing the sought-for currents and voltages along the interconnect structure.

By way of example, the proposed method has been applied to a linearly tapered microstrip line and a pair of coupled lines with random variation of the p.u.l. parameters along the line. In both cases a high accuracy was achieved. Additionally, the importance of employing a *two-step* perturbation to get sufficient accuracy for the transmission coefficients was highlighted. Consideration of the computational time of the perturbation approach showed improved efficiency w.r.t. the reference chain parameter matrix method.

References

[1] L. A. Hayden and V. K. Tripathi, "Nonuniformly coupled microstrip transversal filters for analog signal-processing," *IEEE Trans. Microw. Theory Tech.*, vol. 39, no. 1, pp. 47–53, Jan. 1991.

[2] R. N. Ghose, "Exponential transmission lines as resonators and transformers," *IEEE Trans. Microw. Theory Tech.*, vol. 5, no. 3, pp. 213–217, Jul. 1957.

[3] P. Salem, C. Wu, and M. Yagoub, "Non-uniform tapered ultra wideband directional coupler design and modern ultra wideband balun integration," in *Asia Pacific Microw. Conf., Yokohama, Japan*, Dec. 2006, pp. 891–894.

[4] T. Dhaene, L. Martens, and D. De Zutter, "Transient simulation of arbitrary nonuniform interconnection structures characterized by scattering parameters," *IEEE Circuits Syst. Mag.*, vol. 39, no. 11, pp. 928–937, Nov. 1992.

[5] Y.-W. Hsu and E. F. Kuester, "Direct synthesis of passband impedance matching with nonuniform transmission lines," *IEEE Trans. Microw. Theory Tech.*, vol. 58, no. 4, pp. 1012–1021, Apr. 2010.

[6] P. Rulikowski and J. Barrett, "Application of nonuniform transmission lines to ultra wideband pulse shaping," *IEEE Microw. Wireless Compon. Lett.*, vol. 19, no. 12, pp. 795–797, Dec. 2009.

[7] B. Curran, I. Ndip, S. Guttowski, and H. Reichl, "A methodology for combined modeling of skin, proximity, edge, and surface roughness effects," *IEEE Trans. Microw. Theory Tech.*, vol. 58, no. 9, pp. 2448–2455, Sep. 2010.

[8] L. Vegni, F. Urbani, and A. Toscano, "Exponentially tapered non uniform transmission lines," *IEEE Trans. Magn.*, vol. 33, no. 2, pp. 1492–1495, Mar. 1997.

[9] C. Edwards, M. Edwards, S. Cheng, and C. C. Stitwell, R. K. Davis, "A simplified analytic CAD model for linearly tapered microstrip lines including losses," *IEEE Trans. Microw. Theory Tech.*, vol. 52, no. 3, pp. 823–830, Mar. 2004.

[10] J. Nitsch and F. Gronwald, "Analytical solutions in nonuniform multiconductor transmission line theory," *IEEE Trans. Electromagn. Compat.*, vol. 41, no. 4, pp. 469 – 479, Nov. 1999.

[11] M. Tang and J. F. Mao, "A precise time-step integration method for transient analysis of lossy nonuniform transmission lines," *IEEE Trans. Electromagn. Compat.*, vol. 50, no. 1, pp. 166–174, Feb. 2008.

[12] Q. Xu and P. Mazumder, "Accurate modeling of lossy nonuniform transmission lines by using differential quadrature methods," *IEEE Trans. Microw. Theory Tech.*, vol. 50, no. 10, pp. 2233–2246, Oct. 2002.

[13] C. R. Paul, *Analysis of Multiconductor Transmission Lines*. John Wiley & Sons, 1994.

[14] J. F. Mao and Z. F. Li, "Analysis of the time response of nonuniform multiconductor transmission lines with a method of equivalent cascaded network chain," *IEEE Trans. Microw. Theory Tech.*, vol. 40, no. 5, pp. 948–954, May 1992.

[15] N. Orhanovic, P. Wang, and V. K. Tripathi, "Time-domain simulation of uniform and nonuniform multiconductor lossy lines by the method of characteristics," *IEEE Trans. Comput.-Aided Design Integr. Circuits Syst.*, vol. 12, no. 6, pp. 900–904, Jun. 1993.

[16] J. F. Mao and Z. F. Li, "Analysis of the time response of multiconductor transmission lines with frequency-dependent losses by the method of convolution-characteristics," *IEEE Trans. Microw. Theory Tech.*, vol. 40, no. 4, pp. 637–644, Apr. 1992.

[17] M. Khalaj-Amirhosseini, "Analysis of coupled nonuniform transmission lines using Taylor's series expansion," *IEEE Trans. Electromagn. Compat.*, vol. 48, no. 3, pp. 594–600, Aug. 2006.

[18] ——, "Analysis of lossy inhomogeneous planar layers using Fourier series expansion," *IEEE Trans. Antennas Propag.*, vol. 55, no. 2, pp. 489–493, Feb. 2007.

[19] F. Y. Chang, "Waveform relaxation analysis of nonuniform lost transmission lines characterized with frequency dependent parameters," *IEEE Trans. Circuits Syst.*, vol. 38, no. 12, pp. 1484–1500, Dec. 1991.

[20] E. Gad and M. Nakhla, "Efficient simulation of nonuniform transmission lines using integrated congruence transform," *IEEE Trans. VLSI Syst.*, vol. 12, no. 12, pp. 1307 –1320, Dec. 2004.

[21] S. Barmada and M. Raugi, "Transient numerical solutions of nonuniform MTL equations with nonlinear loads by wavelet expansion in time or space domain," *IEEE Trans. Circuits Syst. I*, vol. 47, no. 8, pp. 1178 – 1190, Aug. 2000.

[22] S. Javadzadeh, Z. Mardy, K. Mehrany, F. Farzaneh, and M. Fardmanesh, "Fast and efficient analysis of transmission lines with arbitrary non-uniformities of sub-wavelength scale," *IEEE Trans. Microw. Theory Tech.*, vol. 60, no. 8, pp. 2378–2384, Aug. 2012.

[23] M. Khalaj-Amirhosseini, "Analysis of nonuniform transmission lines using the equivalent sources," *Progress In Electromagnetics Research*, vol. 71, pp. 95–107, 2007.

[24] T. Demeester and D. De Zutter, "Quasi-TM transmission line parameters of coupled lossy lines based on the Dirichlet to Neumann boundary operator," *IEEE Trans. Microw. Theory Tech.*, vol. 56, no. 7, pp. 1649–1660, Jul. 2008.

[25] J. G. Van Bladel, *Electromagnetic Fields*. John Wiley & Sons, 2007.

[26] J. J. Goedbloed, *Electromagnetic Compatibility*. Prentice Hall, 1992.

[27] C. Gazda, D. Vande Ginste, H. Rogier, R.-B. Wu, and D. De Zutter, "A wideband common-mode suppression filter for bend discontinuities in differential signaling using tightly coupled microstrips," *IEEE Trans. Adv. Packag.*, vol. 33, no. 4, pp. 969–978, Nov. 2010.

[28] T. Demeester and D. De Zutter, "Construction of the Dirichlet to Neumann boundary operator for triangles and applications in the analysis of polygonal conductors," *IEEE Trans. Microw. Theory Tech.*, vol. 58, no. 1, pp. 116 – 127, Jan. 2010.

[29] D. Vande Ginste, D. De Zutter, D. Deschrijver, T. Dhaene, P. Manfredi, and F. Canavero, "Stochastic modeling-based variability analysis of on-chip interconnects," *IEEE Trans. Compon., Packag., Manuf. Technol. A*, vol. 2, no. 7, pp. 1182–1192, Jul. 2012.

[30] W. Fan, A. Lu, L. L. Wai, and B. K. Lok, "Mixed-mode S-parameter characterization of differential structures," in *5th Electronics Packaging Technology Conference, Singapore*, 2003, pp. 533 – 537.

Mykola Chernobryvko was born in 1987. He received the M.S. degree in electronic engineering from Kharkiv National University of Radioelectronics, Kharkiv, Ukraine, in 2009. He is currently a Doctoral Researcher at the Department of Information Technology at Ghent University. His research interests comprise electromagnetic modeling of interconnects and signal integrity.

Dries Vande Ginste was born in 1977. He received the M.S. degree and the Ph.D. degree in electrical engineering from Ghent University, Gent, Belgium, in 2000 and 2005, respectively. He is currently an Assistent Professor with the Electromagnetics Group, Department of Information Technology, Ghent University. In June and July 2004, he was a Visiting Scientist at the Department of Electrical and Computer Engineering, University of Illinois at Urbana-Champaign (UIUC), IL, USA. From September to November 2011, he was a Visiting Professor at the EMC Group, Dipartimento di Elettronica, Politecnico di Torino, Italy.

His current research interests comprise computational electromagnetics, electromagnetic compatibility, signal and power integrity, and antenna design. Dr. Vande Ginste was awarded the International Union of Radio Science (URSI) Young Scientist Award at the 2011 URSI General Assembly and Scientific Symposium and he received the Best Poster Paper Award at the 2012 IEEE Electrical Design of Advanced Packaging and Systems Symposium (EDAPS). He is a Senior Member of the IEEE.

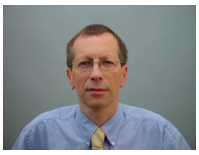

Daniël De Zutter was born in 1953. He received his M. Sc. Degree in electrical engineering from the University of Gent in 1976. In 1981 he obtained a Ph. D. degree and in 1984 he completed a thesis leading to a degree equivalent to the French Aggrgation or the German Habilitation. He is now a full professor of electromagnetics. His research focusses on all aspects of circuit and electromagnetic modelling of high-speed and high-frequency interconnections and packaging, on Electromagnetic Compatibility (EMC) and numerical solutions of Maxwell's equations. As author or co-author he has contributed to more than 200 international journal papers (cited in the Web of Science) and 200 papers in conference proceedings. In 2000 he was elected to the grade of Fellow of the IEEE. He was an Associate Editor for the IEEE Microwave Theory and Techniques Transactions. Between 2004 and 2008 he served as the Dean of the Faculty of Engineering of Ghent University and is now the head of the Department of Information Technology.